CHINESE JOURNAL OF PHYSICS VOL. 52, NO. 1-I February 2014

Synthesis, Photoluminescence, and Magnetic Properties of Arrayed Al Doped $Zn_{0.95}Co_{0.05}O$ Nanorods

Y. M. Liu,* M. Li, Q. Q. Fang, Q. R. Lv, M. Z. Wu, Z. Q. Sun, X. P. Song, and G. He

School of Physics and Materials Science,
The Key Laboratory of Information Materials and Devices,
Anhui University, Hefei 230601, China
(Received February 7, 2013)

Arrayed $Zn_{0.95-x}Al_xCo_{0.05}O$ (ZnAlCoO for $x = 0.02$–0.07 and ZnCoO for $x = 0$) nanorods have been synthesized by a low temperature hydrothermal method and characterized as ZnO hexagonal structures by their X-ray diffraction (XRD) spectra, Raman spectra, and scanning electron microscopy (SEM), which show that Al doping can modulate the density and the cross section shape of the ZnCoO nanorods. Al and Co atoms substituting for Zn atoms in ZnAlCoO samples were successfully doped into a ZnO lattice, which has been characterized by X-ray photoelectron spectroscopy (XPS) and photoluminescence (PL) spectra. PL spectra exhibit that Al doping in ZnCoO markedly enhanced the visible light emission (VL) while it depressed the ultraviolet emission (UV). The positions of the UV peak first redshifted from 386 to 387 nm, then blueshifted to a shorter wavelength side (374 nm) with increasing Al doping concentration. Moreover, VL appears with redshifts and a maximum of intensity for the middle Al doping ($x = 0.04$) sample. The high Al ($x = 0.07$) doping sample exhibits room temperature ferromagnetism (RTFM) with saturation magnetization 20 times larger than that of the middle Al ($x = 0.04$) doping sample while the low Al doping ($x = 0.02$) sample exhibits no RTFM. The above structural, optical and magnetic phenomena are all discussed.

DOI: 10.6122/CJP.52.286 PACS numbers: 81.07.-b, 78.55.Et, 75.50.Pp, 61.05.cp

Due to its wide direct band gap of 3.37 eV at room temperature, exclusive properties, and potential applications in the nano-device field, one-dimensional (1D) nano-structured ZnO has attracted much attention [1, 2]. Its large free exciton binding energy (60 meV) ensures an efficient emission up to room temperature and makes it suitable for short wavelength optoelectronic applications, while the intense and stable visible luminescence can make ZnO nanorods an efficient phosphor [3]. The large surface area of the nanorods makes them attractive for gas and chemical sensing, and the ability to control their nucleation sites makes them candidates for micro-lasers or memory arrays. So the functional design of nano-materials in a highly oriented and ordered array is crucial for the next generation device design [4].

Doping of transition metals is an effective method for adjusting the energy levels and the surface states of ZnO, which can further lead to changes in the electrical, optical, and magnetic properties of ZnO by which dilute magnetic semiconductors (DMSs) can be realized. DMSs have shown a potential because they not only have semiconducting properties but also magnetic properties. Semiconducting properties permit electrical devices

*Electronic address: lymf@sina.com.cn

to be operated effectively and promptly, and magnetic properties make enormous data storage possible. Therefore, DMSs can be used for the rapid processing and superior storage of information at the same time [5]. Co dopant is usually used for magnetism doping [6]. It is a challenge to achieve highly conducting Co doped ZnO films without degrading their magnetic properties, as substitution of Co often leads to an increase in the resistivity of the films. ZnO has n type electron conductivity with an appropriate dopant such as Al or Ga [7]. Recent reports correlated the magnetic moment with the carrier concentration in Co or (Co, Al) doped films [8, 9], but no intrinsic relation between the magnetization and electron concentration have been observed in Al-doped $Zn_{0.95}Co_{0.05}O$ films [10]. Liu *et al.* concluded that the intentional donor doping plays an important role in realizing dominant ferromagnetic ordering in Co-doped ZnO films, while Alaria *et al.* found the absence of ferromagnetism in Al-doped Zn0.9Co0.10O diluted magnetic semiconductors [11, 12]. Jayakumar *et al.* also indicated that low Al doping played little role in (Co, Al) co-doped ZnO [13].

Al doping in ZnO can modify the photoluminescence of ZnO which is related to defects [14, 15]. It has been reported that when Al was doped into thin films, the deep level (DL) emissions of the thin films were suppressed [16]. The effect of Al doping on the photoluminescence of ZnCoO was little reported. Herein, based on the above and the disagreement on the ferromagnetism of ZnCoO, the effects of Al doping on ZnCoO should be further studied.

ZnO nanorod arrays have been synthesized by different methods, such as chemical vapor deposition (CVD), pulsed laser deposition (PLD), solution synthesis, and so on [17, 18]. More attention has been paid on the hydrothermal method of synthesizing nanorod arrays due to its low cost and convenience since Vassieres first successfully synthesized ZnO nanorod arrays [4]. It has been evidenced that the doping in ZnO by the low temperature hydrothermal method is an efficient method [19]. In this paper, the characterization of the morphologies and structures of Al doped ZnCoO films indicates that the hydrothermal method at low temperature is not only economical but also effective for two or more elements-codoping in arrayed ZnCoO nanorods. The two or more elements-codoping in ZnO nanorod arrays fabricated by the solution method has not been reported. Here, we successfully synthesized arrayed $Zn_{0.95-x}Al_xCo_{0.05}O$ nanorods via the hydrothermal method and studied the effects of Al doping on their structures, photoluminescence, and magnetic properties, demonstrating that Al doping can obviously enhance the parallel growth, the RTFM, and the VL emission of ZnCoO nanorods, while reducing their UV emission.

An appropriate quantity of ammonia (25%) and 0.1 M zinc nitrate, aluminum nitrate and cobalt nitrate aqueous solution were mixed and stirred vigorously for ten minutes to form a homogeneous solution. Ammonia was used to adjust the pH value of the mixture to 9. The resulting solutions was then transferred into a Teflon-lined autoclave, which was sealed and maintained at 70 °C for 10 h, then left to cool to room temperature naturally. A light brown layer of precipitate was deposited on the glass covered with a ZnO seed layer which was prepared by spin coating [20]. After being washed with deionized water several times, the as-obtained sample was finally dried at 115 °C for 2 h for further characterization. According to the above procedures, three samples can be obtained by changing the ratio

of Zn to Al from 93:2 to 91:4, then to 88:7 in the above mentioned initial mixture solution while keeping the Co nominal concentration invariable, i.e., $Zn_{0.95-x}Al_xCo_{0.05}O$ (ZnAlCoO, $x = 0.02$, 0.04, and 0.07) which were labeled as ZCA2, ZCA4, and ZCA7, respectively. The Al doping concentration is denoted by x, and the nominal doping concentration of the Co ions is 0.05. For comparison, a $Zn_{0.95}Co_{0.05}O$ nanorods array (labeled as ZC5) was prepared at the similar condition as the ZnAlCoO nanorods arrays without aluminum nitrate in existence in the source solution.

The images and crystal structures of the above samples have been characterized by a scanning electron microscope (SEM Hitachi S-4800) and X-ray diffraction (XRD MAP18AHF) using the Cu Kα line under the excitation voltage of 40 kV and tube current of 50 mA, respectively. The photoluminescence and Raman spectra (PL LabRAM-HR) were measured under the excitation of a He-Cd laser using the wavelength of 325 nm and an Ar^+ laser with 515 nm, respectively, at room temperature. Room magnetic properties were obtained by a Vibrating Sample Magnetometer (BHV255). Sample ZCA7 was also characterized by X-ray photoemission spectroscopy (XPS ESCALAB250) using Al Kα.

Figure 1 presents the plane view SEM images of the ZnAlCoO nanorods arrays, from which it can be seen that the alignment growth of the nanorods vertical to the substrate was markedly enhanced, and the average diameter of the nanorods increases from 100 nm to 200 nm when the Al doping concentration was increased from 0.02 to 0.04. Further increasing Al to 0.07, the average diameter of the nanorods decreases to 100 nm, the nanorod density increases obviously. The increase of Al doping concentration in ZnCoO markedly enhanced the densities of the arrayed nanorods, which is different from the effect of Al ions in a ZnO reaction solution in the literature [21], meaning that Al doping leads to the enhancement of the nucleation rate of the nanorods in a ZnAlCoO reaction solution. Therefore, the increase of Al dopant in ZnAlCoO reaction solution corresponds to increasing the degree of supersaturation of the reaction solution.

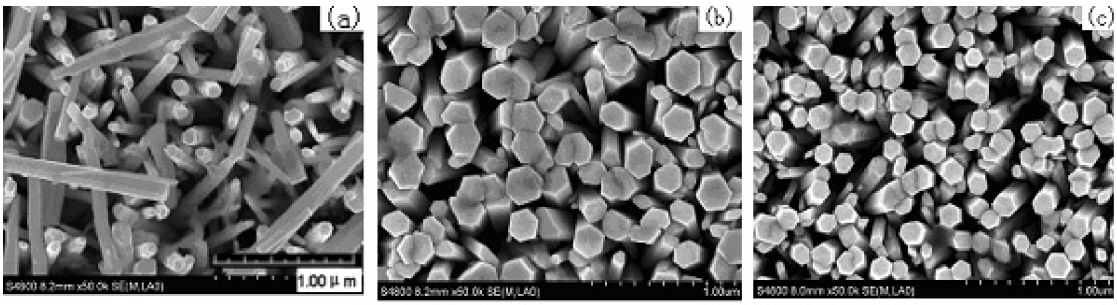

FIG. 1: The plane view SEM images of sample (a) ZCA2, (b) ZCA4, and (c) ZCA7.

It is worth noting that the nanorods with screw growth tips in Figure 1(a) are not uniform in diameter, while the cross sections of the nanorods in Figure 1(b) are less regular than that of the nanorods in Figure 1(c), which may be merged by two or more nanorods. The reaction solution concentration related morphology changes of ZnO have been observed by Liang *et al.*, which were explained by the dislocation-driven growth mechanism [22]. The

above shape changes of the ZnAlCoO nanorods with Al doping concentration can also be understood by the dislocation-driven growth mechanism, due to Al doping having similar effects on the degree of supersaturation of reaction solutions with an increase of reaction solution concentration.

From the XRD spectra of the samples shown in Figure 2 it can be clearly seen that all diffraction peaks match that of ZnO, indicating that (Co, Al) codoping cannot change the hexagonal structures of ZnO nanorods. Moreover, a (002) diffraction peak dominates all spectra of the ZnAlCoO nanorods arrays, showing that the nanorods in all samples almost grew in alignment along the [001] direction and (Co, Al) codoping cannot change the growth habit of ZnCoO nanorods. Compared with that of ZnCoO, the (002) peak positions of the ZnAlCoO nanorods arrays shift to the high angle direction in the inset of Figure 2, corresponding to lattice shrinkage of the ZnAlCoO nanorods as the Bragg equation ($2d\sin\theta = \lambda$, d denotes crystal plane interval) indicated, meaning that Al and Co atoms substituting for Zn were doped into the ZnCoO lattice, because the radius of an Al ion (0.039 nm) is smaller than that of a Co ion (0.058 nm) and Zn ion (0.060 nm) [23]. It is also found that the (002) diffraction peaks of all the samples are asymmetrical with the (002) shoulder peaks at the higher angle sides, which can be ascribed to $\lambda_{K\alpha 2}$ diffraction of the (002) plane [24].

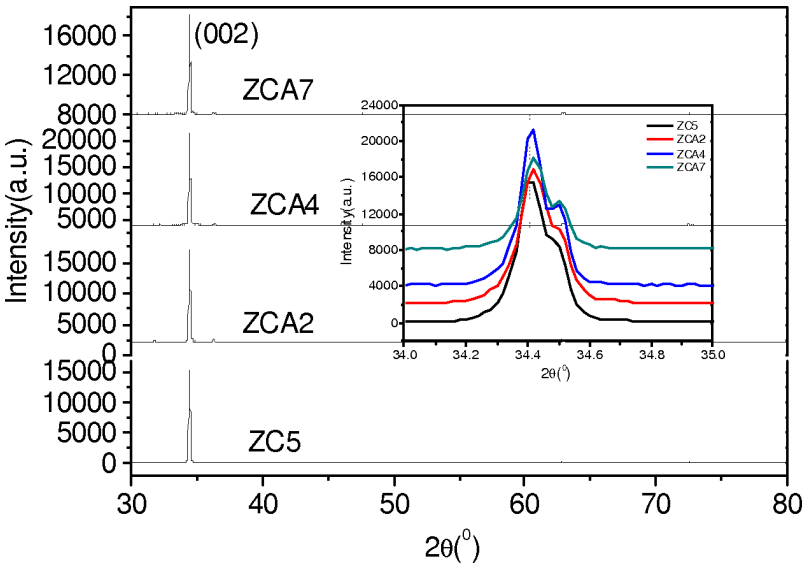

FIG. 2: XRD spectra of ZC5, ZCA2, ZCA4, and ZCA7, and the enlarged patterns of (002) peaks in the inset.

Figure 3 presents the Co2p, Al2p, Zn2p, and O1s core level XPS spectra of ZCA7. The charge-shifted spectra were corrected using the maximum of the adventitious C1s signal at 284.6 eV. The Co2p3/2 peak is at 780.8 eV, while the Co2p1/2 peak at 796.7 eV as shown in Fig. 3(a). The existence of the resonant shake up satellite peaks along with the Co2p doublets at the higher energy side suggests that Co is in a high spin state (Co^{2+}) in the

ZnAlCoO nanorods [25].

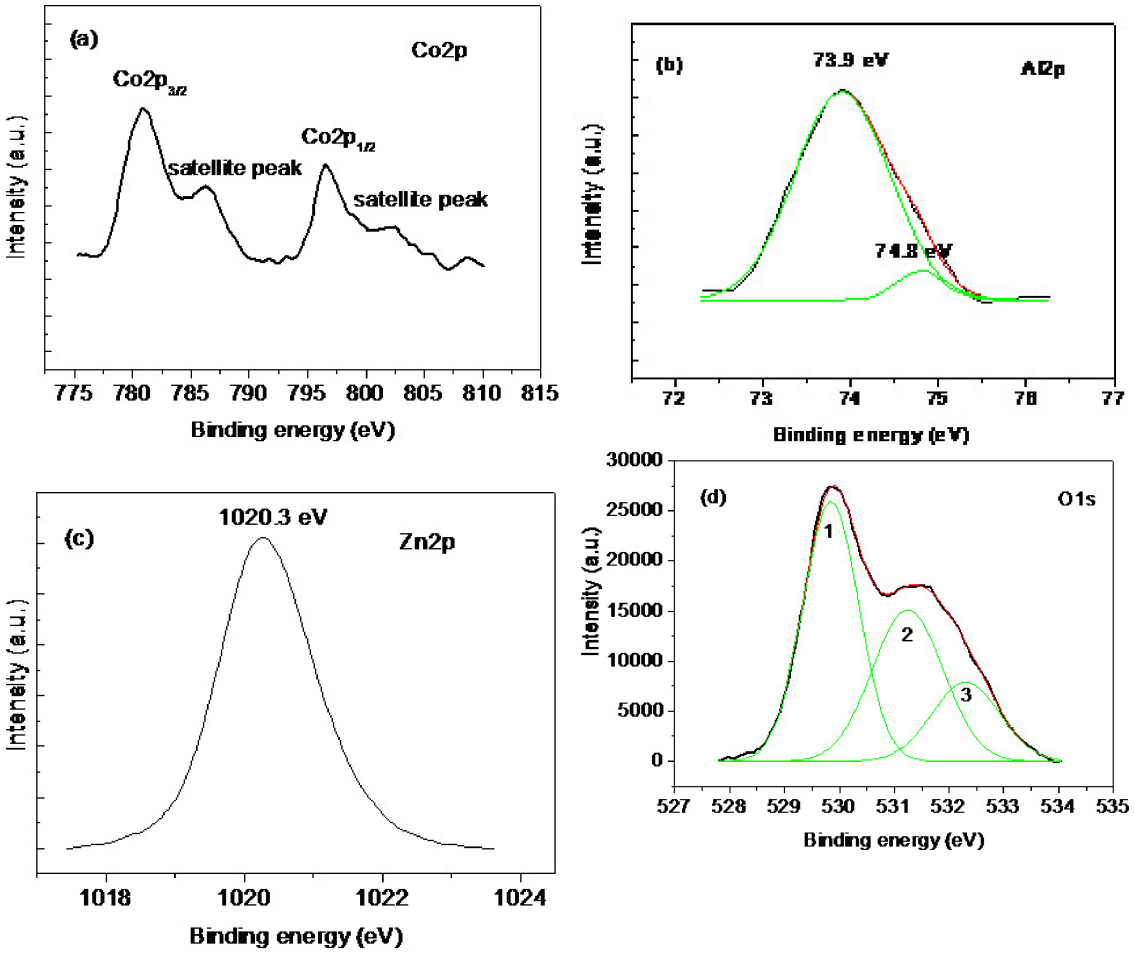

FIG. 3: The core level XPS spectra of ZCA7: (a) Co2p, (b) Al2p, (c) Zn2p, and (d) O1s; (a) Co2p spectrum; (b) Al2p spectrum (black line) decomposed into two peaks (green line) by Gaussian fitting (red line); (c) Zn2p spectrum; (d) O1s spectrum (black line) decomposed into three peaks (green line) by Gaussian fitting (red line).

Fig. 3 (b) shows the typical XPS data of Al2p3/2 in the ZCA7 sample. The Al2p3/2 peak exhibits an asymmetry feature, which can be divided into two subpeaks at 73.9 eV and 74.8 eV respectively by Gaussian fitting. The Al2p core-level of Al doped ZnO thin films was observed to be present at around 72.6 eV [26]. The Al2p3/2 peak at 74.4 eV in Al-N codoped ZnO films was thought to be caused by the formation of Al-2N binding bonds [27]. In our work, the Al2p3/2 peak appears at higher energies relative to 72.6 eV, suggesting that the Co^{2+} and Al^{3+} ions substituting for Zn ions were inserted into the ZnO matrix and Al^{3+} ions are near Co^{2+} ions, having a lower electron density than that near Zn ions due to the electro-negativity of Co (1.88) being higher than that of Zn (1.65) [28]. Therefore,

the Al binding energy shifting toward higher energy indicates that Co and Al have a strong coupling effect, and a higher binding energy at 74.8 eV may be attributed to the formation of Al-O-Co bonding clusters. The Zn2p3/2 peak of ZCA7 in Fig. 3(c) is symmetric with a lower energy position of 1020.3 eV compared with that of ZC5 (1021.2 eV, not shown here), meaning that Zn^{2+} ions have a single value state and Al ions were successfully doped into the lattice of ZnO due to the electro-negativity of Al (1.61) being lower than that of Zn. The above results also imply that an increase of Al doping concentration in the ZnAlCoO samples corresponding to diluting Co ions will enhance the distances between Co ions.

The O1s peak can be deconvoluted into three peaks with Gaussian line shapes lying at 529.6 eV, 531.0 eV, and 532.1 eV, respectively, as shown in Fig. 3(d). Peak 1 with the lowest energy and peak 3 with the highest binding energy are related to oxygen atoms in the crystal lattice and chemical absorption oxygen atoms, respectively, while peak 2 with the middle binding energy is related to oxygen vacancy defects [29]. Peak 2 has a higher intensity than that of ZC5 (not shown here), indicating that (Co, Al) codoping brings about considerable oxygen vacancy defects.

According to the XPS spectra of ZCA7 and the paper [24], Co and Al factual doping concentrations can be calculated to be 0.05 and 0.07, respectively, which is in agreement with their nominal ingredients.

The Raman spectra for the above four samples are present in Figure 4, in which the peaks located at 98 cm^{-1}, 437 cm^{-1}, and 574 cm^{-1} for the samples can be observed, corresponding to the E2 (low), E2 (high), and A1 (LO) modes of ZnO, respectively [30].

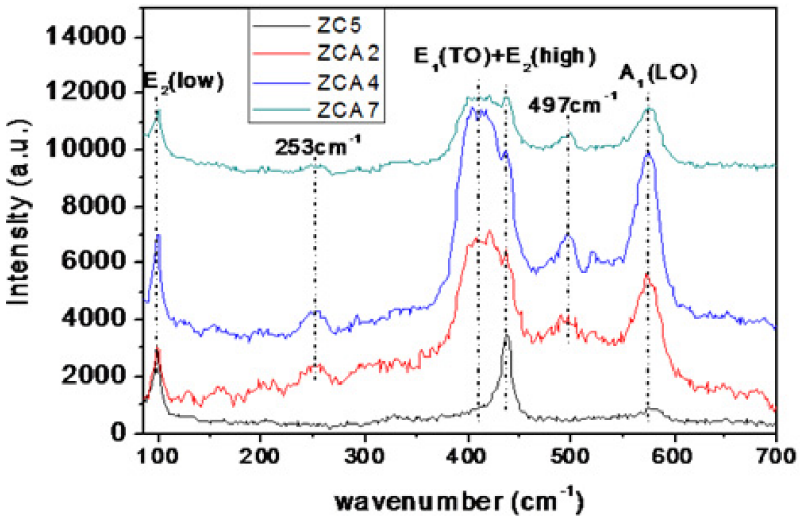

FIG. 4: Raman spectra of ZC5, ZCA2, ZCA4, and ZCA7

As the E2 (high) peak is the characteristic peak of the ZnO hexagonal structure, the existence of E2 (high) peaks in the samples indicates that ZnCoO and Al doped ZnCoO nanorods are hexagonal structures [31]. Their positions do not change with increasing Al doping concentration, which means that there are no stresses in the Al doped ZnCoO lattices

compared with ZnCoO. The A1 (LO) peaks at 574 cm^{-1} are attributed to O vacancies (Vo) etc. defects related to Raman scattering [32]. The redshifts of the A1 (LO) peaks of ZnAlCoO relative to that of ZnCoO have been observed, which were attributed to vacancies related defects [33]. The intensities of A1 (LO) for the ZnAlCoO samples are much higher than that of ZnCoO, supporting the fact that Al and Co codoping greatly increases the intrinsic defects of the ZnO lattice, which will be confirmed by the PL spectra. The peak at 497 cm^{-1} is usually ascribed to the multi-phonon scattering process of a disordered lattice, and the peak at 253 cm^{-1} (B2 mode) can be considered to result from Al doping in ZnAlCoO nanorods enhancing a built-in electric field [34]. Especially to be noticed, in comparison with the ZnCoO sample, all ZnAlCoO samples present a broadened peak which contains E2 (high) peak and a peak centering at 410 cm^{-1}. As the E1 (TO) of ZnO is at 410 cm^{-1}, it is reasonable to think that the broadened peaks are E1 (TO) of ZnAlCoO. The E1 (TO) peak has been observed in Al doped ZnO and reflects the strength of polar lattice bonds [33, 35]. As E1 (TO) is usually related to the oscillation of the atoms on the ab plane, the incorporation of Al atoms into the ZnCoO lattice induces more defects, which relax the stress in the ab plane induced by the replacement of Al for Zn atoms, the vibration of the atoms on the ab plane will enhance, which thus intensifies the E1 (TO) peak. Therefore, the appearance of the E1 (TO) peak induced by Al doping in ZnCoO means that Al doping enhanced the strength of polar lattice bonds.

Photoluminescence spectra are usually used to characterize the defects in nanomaterials. Figure 5 shows the photoluminescence spectra, all of which are composed of near band edge emission (NBE) or ultraviolet light emission (UV) and visible light emission (VL). It is usually thought that UV results from exciton or band-to-band (free-electron to free-hole) transitions and the visible light (VL) from the deep level defect transitions [36].

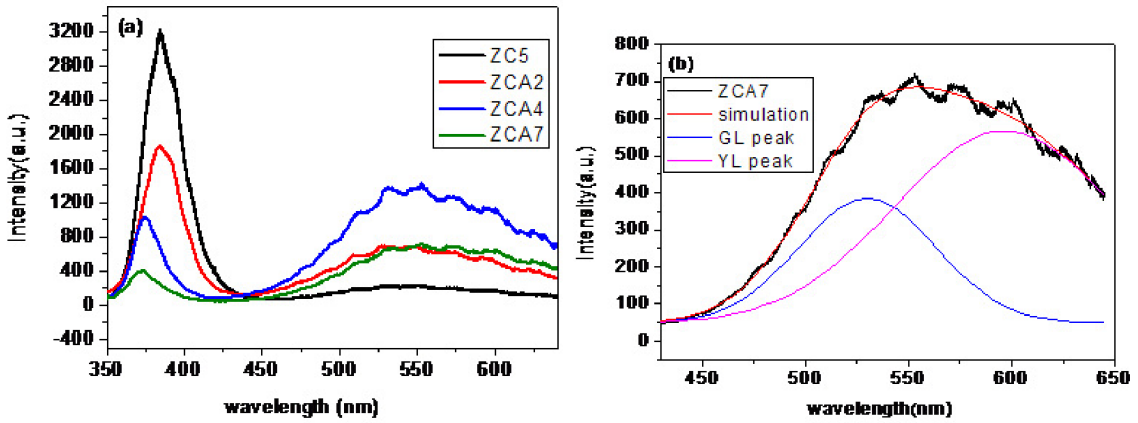

FIG. 5: (a) Photoluminescence spectra of ZC5, ZCA2, ZCA4, and ZCA7; (b) The VL band (black line) decomposed into two peaks corresponding to green light emission (GL, blue line) and yellow light emission (YL, purple line) by Gaussian fitting (red line) for sample ZCA7.

It can be clearly seen from Figure 5 that Al doping in ZnCoO obviously changed the position of the UV peak, which first redshifts then blueshifts, as shown in Table I. With

the Al doping concentration increasing from 0.04 to 0.07, the UV emission peak blueshifts from 387.1 to 374.2 nm, which is usually believed to be induced by the Burstein-Moss (BM) widening effect. The band gap narrowing (BGN) effect dominates when the carrier concentration is lower than the critical value of the BM effect, due to the electron-electron repulsive interaction [37]. Here, the BGN and BM effect observed in Al doped ZnCoO mean that more carriers were induced with increasing Al doping concentration.

TABLE I: The dependence of the peak positions of UV, GL, and YL, and the ratios of UV intensity to VL intensity (I_{UV}/I_{VL}), I_{GL}/I_{VL}, and I_{YL}/I_{VL} on Al doping concentration.

Al doping conrentration	UV/nm	GL/nm	YL/nm	I_{UV}/I_{VL}	I_{GL}/I_{VL}	I_{YL}/I_{VL}
0	386.3	525.9	573.9	0.74	0.32	0.68
0.02	387.1	526.0	583.1	0.12	0.31	0.69
0.04	376.8	528.4	591.6	0.05	0.30	0.70
0.07	374.2	530.0	596.4	0.09	0.29	0.71

In Figure 5, Al doping continuously decreases the intensities of UV while it obviously increases the intensities of VL centered at about 550nm, leading to the decrease of the ratio of intensity of UV to that of VL, as shown in Table I, which indicates the formation of Al-O bonds and localized Al-impurity states in ZnAlCoO [15]. The wide peak at 550 nm has also been observed in ZnO nanostructures by researchers, and is considered to be jointly caused by different deep energy level defects [38]. In this paper, the wide VL peak can be deconvoluted into two bands by Gaussian fitting, which are a green light emission (GL) band centered at 530 nm and a yellow light emission (YL) band at 596 nm for ZCA7, as indicated by Fig. 5(b). The GL and YL peak positions for the four samples are shown in Table I derived from Figure 5(a). GL is usually thought to be related to the electron transitions from singly ionic oxygen vacancies (V_O^+) related energy states to the valence band [39]. YL is usually attributed to oxygen interstitials (O_i) or V_{Zn} related transitions [40, 41]. Al ions with valence value of +3 and Co^{2+} ions codoped into the ZnO lattice substituted for Zn^{2+} ions, which will bring about charge imbalance. To make the charges balance, the crystal lattice will form compensating defects, such as V_{Zn} or O_i etc. accepter defects. Therefore, the YL intensity relative to GL increases with Al doping content increasing from 0.02 to 0.07, as indicated by Table I, implying that Al doping induced more acceptor defects than V_O defects to compensate for the charge imbalance induced by the incorporation of Al in ZnCoO with the increase of Al dopant.

From Fig. 5(a), it also can be seen that for VL the intensity first increases then decreases with increasing Al doping content, which means that the defect concentration reaches saturation in ZCA4, and a further increase of Al dopants leads to neutralization between the acceptor defects and V_O^+ donor defects, decreasing the VL intensity. According to the change trend of the VL intensity with Al doping concentration, we can deduce that the acceptor defects should be O_i defects, which can neutralize V_O^+ defects. The redshifts of the YL and GL positions with the increase of the Al doping concentration can be observed

in Table I. The redshift of YL has been reported in Mg doped ZnO, which results from the wider energy level distribution of O_i defects [42]. Hur *et al.* proposed that the electron charge transfer from the localized impurity state to the effective band is accomplished by the potential fluctuation of the Al-impurity potential in the excitation process, which contributes to the VL intensity [43]. With increasing charge compensation and impurity concentration, the localized impurity potential well deepens, due to reduced screening of the potential fluctuations [44]. Therefore, the redshift of YL and GL can be considered to be from the deepening of the Al impurity potential well. Moreover, GL is related to the transition from the Al impurity potential related V_{O}^{+} energy level to the valence band, while YL is related to the transition from the Al impurity potential to the O_i defects. Further studies on the redshifts of VL are also needed.

Figure 6 shows the magnetic curves of ZC5, ZCA2, ZCA4, and ZCA7, from which it can be seen that the ZCA4 and ZCA7 samples present room temperature ferromagnetism, and the saturation magnetization of ZCA7 is nearly 20 times larger than that of ZCA4. ZC5 and ZCA2 exhibit no magnetism.

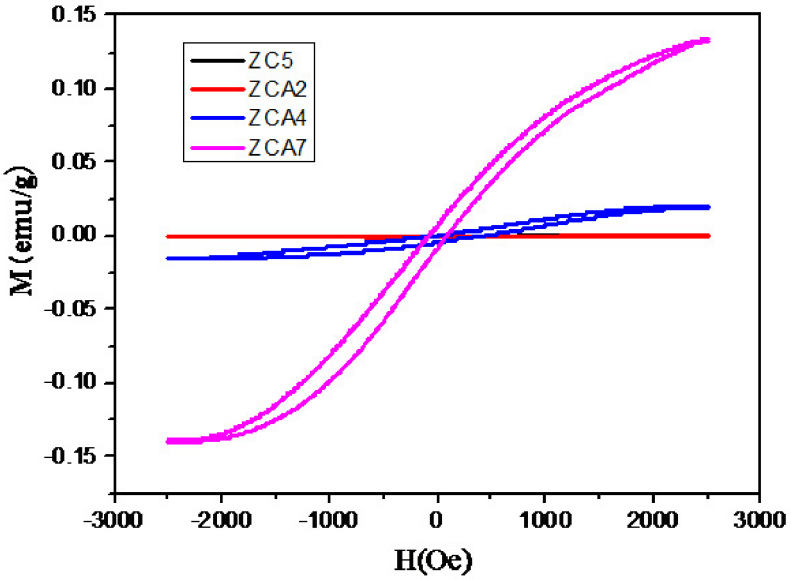

FIG. 6: Magnetic curves of ZC5, ZCA2, ZCA4, and ZCA7

Chang *et al.* thought that the ferromagnetism in (Co,Al) co-doped ZnO semiconductors mainly arises from the hybridization of Al interstitial defects with Co substitutional dopants, and Belghazi showed that no change in the magnetic properties of ZnCoO with Al doping was to be ascribed to no overlap between the Al and the Co states [45, 46]. Indirect interaction of Co^{2+} leads to ferromagnetism, whereas direct interaction of Co^{2+} can result in antiferromagnetism [47]. With an increase of the Al doping concentration, the average distance between Co^{2+} ions and the hybridization of Al related defects and Co substitutional dopants increase, leading to the enhancement of the ferromagnetic contribution to

the ZCA4 and ZCA7 samples.

The bound magnetic polaron (BMP) model [5, 48] and RKKY interaction (or carrier mediated FM) [49, 50] are usually used to explain the FM of ZnO-based nanostructures. The ferromagnetism of Co doped ZnO nanostructures has also been ascribed to be oxygen vacancy modulated [5]. ZCA4 has weaker ferromagnetism compared with ZCA7, while it has the largest vacancy concentration for the four samples. This means that the BMP model cannot explain the ferromagnetisms observed in ZCA4 and ZCA7. Low carrier concentration and the shorter distances between magnetic ions may be the reason of no magnetism for ZC5 and ZCA2. With the Al doping concentration increasing up to 0.04, the distances between the Co ions and free carriers increase, as reflected by the shifts of the UV band, resulting in the enhancement of the ferromagnetic interaction between Co ions. As a result, ZCA4 exhibits ferromagnetism. Combined with the larger distances between Co ions, the increased carrier concentrations in ZCA7, and the enhanced coupling effect of Co and Al ions, it is readily understood that the remarkable increase of the saturation magnetization of the ZCA7 sample in comparison with that of ZCA4 results from a carrier mediated ferromagnetism mechanism [9].

In conclusion, the arrayed Al doped ZnCoO ($Zn_{0.95-x}Al_xCo_{0.05}O$, $x = 0.02 - 0.07$) nanorods arrays were synthesized via the hydrothermal method at 700 C. The analysis results indicate that Al doping can modulate the density and the cross section shape of ZnAlCoO nanorods with hexagonal structure. XPS imply that Co and Al atoms substituting for Zn have been successfully doped into ZnO crystal lattice, and appropriate Al dopants in ZnAlCoO will modulate the distances between Co ions. In the Raman spectra, a broadened E1 (TO) peak and markedly enhanced A1 (LO) peak in ZnAlCoO samples have been observed, which is a clue to the enhancement of the strength of the polar lattice bonds and more O related defects induced by Al doping.

By analyzing the PL spectra, conclusions can be drawn that Al doping enhanced the electron carrier concentration, resulting in a shift of the UV peak and induced more O_i compensation defects in the ZnAlCoO samples. The redshifts of the VL positions with the increase of Al doping concentration can be considered from the deepening of the Al impurity potential well. The markedly enhanced VL emission intensity by Al doping in ZnAlCoO will be valuable for white light research and the application of ZnO. With increasing Al concentration up to 0.04, the RTFM of the ZnAlCoO samples starts to be observed, and the ZCA7 sample presents the maximum saturation magnetization, which can be explained by a carrier mediated ferromagnetism mechanism. Al dopants play an important role in enhancing the coupling effect of Co and Co ions.

Acknowledgements

The work was financially supported by the Research Foundation for the Doctoral Program of High Education of China (20093401110004), Anhui Provincial Natural Science Foundation (090414177, 11040606M49, 1208085MF99), National Natural Science Foundation of China (11374013, 51272001) and A Scientific Research Startup Outlay for Doctors

in Anhui University.

References

[1] K. Keren, R. S. Berman, E. Buchstab, U. Sivan, and E. Braun, Science **302**, 1380 (2003). doi: 10.1126/science.1091022
[2] X. D. Wang, J. H. Song, J. Liu, and Z. L. Wang, Science **316**, 102 (2007). doi: 10.1126/science.1139366
[3] J. Nayak, S. Kimura, and S. Nozaki, J. Lumin. **129**, 12 (2009). doi: 10.1016/j.jlumin.2008.07.005
[4] L. Vassieres, Adv. Mater. **15**, 464 (2003).
[5] J. M. D. Coey, M. Venkatesan, and C. B. Fitzgerald, Nat. Mater. **4**, 173 (2005). doi: 10.1038/nmat1310
[6] K. Ueda, H. Tabata, and T. Kawai, Appl. Phys. Lett. **79**, 988 (2001). doi: 10.1063/1.1384478
[7] A. J. Behan *et al.*, Phys. Rev. Lett. **100**, 047206 (2008). doi: 10.1103/PhysRevLett.100.047206
[8] X. C. Liu *et al.*, Appl. Phys. Lett. **88**, 252503 (2006). doi: 10.1063/1.2216887
[9] L. Liao *et al.*, J. Appl. Phys. **102**, 114307 (2007). doi: 10.1063/1.2815629
[10] M. Venkatesan Appl. Phys. Lett. **90**, 242508 (2007). doi: 10.1063/1.2748343
[11] X. C. Liu *et al.*, J. Cryst. Growth **307**, 14 (2007).
[12] J. Alaria, H. Bieber, S. Colis , G. Schmerber, and A. Dinia, Appl. Phys. Lett. **88**, 112503 (2006). doi: 10.1063/1.2186079
[13] O. D. Jayakumar *et al.*, Nanoscale **2**, 1505 (2010). doi: 10.1039/c0nr00195c
[14] S. Yun, J. Lee, J. Yang, and S. Lim, Physica B **405**, 413 (2010). doi: 10.1016/j.physb.2009.08.297
[15] S. Y. Kuo, W. C. Chen, F. I. Laic, C. P. Cheng, and H. C. Kuo, J. Cryst. Growth **287**, 78 (2006).
[16] Y. X. Liu *et al.*, J. Alloys Compd. **506**, 772 (2010).
[17] J. J. Wu and S. C. Liu, Adv. Mater. **14**, 215 (2002). doi: 10.1002/1521-4095(20020205)14:3<215::AID-ADMA215>3.0.CO;2-J
[18] B. J. Jin, S. Im, and S. Y. Lee, Thin Solid Films **366**, 107 (2000). doi: 10.1016/S0040-6090(00)00746-X
[19] Y. M. Liu *et al.*, J. Phys. D: Appl. Phys. **40**, 4594 (2007).
[20] S. Im, B. J. Jin, and S. Yi, J. Appl. Phys. **87**, 4558 (2000).
[21] M. S. Wang *et al.*, J. Alloys Compd. **507**, L21 (2010).
[22] Z. W. Liang *et al.*, CrystEngComm **14**, 1723 (2012).
[23] S. J. Pearton, D. P. Norton, K. Ip, Y. W. Heo, and T. Steiner, Prog. Mater. Sci. **50**, 293 (2005).
[24] Y. M. Liu *et al.*, Appl. Surf. Sci. **257**, 6540 (2011). doi: 10.1016/j.apsusc.2011.02.074
[25] J. W. Quilty *et al.*, Phys. Rev. Lett. **96**, 027202 (2006). doi: 10.1103/PhysRevLett.96.027202
[26] G. W. Cong *et al.*, Appl. Phys. Lett. **88**, 062110 (2006). doi: 10.1063/1.2171804
[27] G. D. Yuan *et al.*, J. Cryst. Growth **311**, 2341 (2009). doi: 10.1016/j.jcrysgro.2009.01.128
[28] K. Y. Li and D. F. Xue, J. Phys. Chem. A **110**, 11332 (2006). doi: 10.1021/jp062886k
[29] S. Yun, J. Lee, J. Yang, and S. Lim, Physica B **405**, 413 (2010). doi: 10.1016/j.physb.2009.08.297
[30] X. B. Wang, C. Song, K. W. Geng, F. Zeng, and F. Pan, J. Phys. D: Appl. Phys. **39**, 4992 (2006). doi: 10.1088/0022-3727/39/23/014
[31] R. Yousefi and M. R. Muhamada, J. Solid State Chem. **183**, 1733 (2010). doi: 10.1016/j.jssc.2010.05.007

[32] M. Li *et al.*, J. Appl. Phys. **107**, 104117 (2010). doi: 10.1063/1.3298931
[33] N. Ashkenov *et al.*, J. Appl. Phys. **93**, 126 (2003).
[34] M. Tzolov *et al.*, Thin Solid Films **379**, 28 (2000). doi: 10.1016/S0040-6090(00)01413-9
[35] M. S. Jang *et al.*, Curr. Appl. Phys. **9**, 651 (2009).
[36] A. B. Djurisic and Y. H. Leung, Small **2**, 944 (2006).
[37] Y. H. Yang, X. Y. Chen, Y. Feng, and G. W. Yang, Nano Lett. **7**, 3879 (2007). doi: 10.1021/nl071849h
[38] Q. T. Pan *et al.* J. Phys. D: Appl. Phys. **40**, 6829 (2007).
[39] S. Chakrabarti, D. Ganguli, and S. Chaudhure, J. Phys. D: Appl. Phys. **36**, 146 (2003).
[40] X. L. Wu, G. G. Siu, C. L. Fu, and H. C. Ong, Appl. Phys. Lett. **78**, 2285 (2001). doi: 10.1063/1.1361288
[41] Y. W. Heo, D. P. Norton, and S. J. Pearton, J. Appl. Phys. **98**, 073502 (2005). doi: 10.1063/1.2064308
[42] S. B. Fujihara, Y. Ogawa, and A. Kasa, Chem. Mater. **16**, 2965 (2004). doi: 10.1021/cm049599i
[43] T. B. Hur, Y. H. Hwang, and H. K. Kim, J. Appl. Phys. **96**, 1507 (2004). doi: 10.1063/1.1765861
[44] M. Behringer, P. Baume, J. Gutwski and D. Hommel, Phys. Rev. B **57**, 12869 (1998). doi: 10.1103/PhysRevB.57.12869
[45] G. S. Chang *et al.*, J. Phys. : Condens. Matter **21**, 056002 (2009). doi: 10.1088/0953-8984/21/5/056002
[46] Y. Belghazi *et al.*, J. Appl. Phys. **105**, 113904 (2009). doi: 10.1063/1.3137194
[47] J. L. MacManus-Driscollet, N. Khare, Y. Liu, and M. E. Vickers, Adv. Mater. **19**, 2925 (2007). doi: 10.1002/adma.200602215
[48] S. Sharmaetal, J. Cryst. Growth **321**, 19 (2011).
[49] D. J. Priour, E. H. Hwang and S. Das Sarma, Phys. Rev. Lett. **92**, 117201 (2004). doi: 10.1103/PhysRevLett.92.117201
[50] Y. He *et al.*, Phys. Rev. B **78**, 155202 (2008). doi: 10.1103/PhysRevB.78.155202